Shear strength anisotropy of rooted soils

Ali Akbar Karimzadeh[1], Anthony Kwan Leung[1*], Zhiwei Gao[2]

[1]*Department of Civil and Environmental Engineering, Hong Kong University of Science and Technology, Hong Kong SAR, P.R. China.*

[2]*James Watt School of Engineering, University of Glasgow, Glasgow, G12 8QQ, U.K.*

*Corresponding author. Email: ceanthony@ust.hk

Abstract

The shear strength of rooted soils depends on the principal stress direction owing to the anisotropy in soil structure and root system. Existing failure criteria cannot describe the strength anisotropy of rooted soils under general loading conditions because they are mainly based on the test results of direct shear. This study presents a new generalised 3-D anisotropic failure criterion for rooted soils. The model employs the projection of two independent microstructure fabric tensors (soil fabric and root network) on the stress tensor. Twenty-four drained triaxial compression and extension tests were carried out to measure the strength anisotropy of silty sand vegetated with vetiver grass (*Chrysopogon zizanioides* L.) at different overconsolidation ratios and calibrate the material parameters for the proposed criterion. Anisotropies of both cohesion and friction angle exist in rooted soil. Roots contribute mainly to the increase in cohesion (hence root cohesion) from most of the direct shear test data. Roots with predominant orientation aligning in the tensile strain direction contribute the most to soil strength. In the case of vetiver grass, which has a taproot system, their roots show the strongest reinforcement effect in conventional triaxial extension path, in which the maximum portion of roots are subjected to tension.

Keywords: fabric anisotropy, vegetation, failure criterion, shear strength, soil

Introduction

Plant roots increase soil shear strength (Stokes et al., 2014) through mechanical root reinforcement (Liang et al., 2017; Yildiz et al., 2018; Karimzadeh et al., 2021) and hydrological reinforcement arising from the matric suction induced by root water uptake (Boldrin et al., 2018a; Leung et al., 2019; Mahannopkul & Jotisankasa, 2019; Yildiz et al., 2019), as well as changes in soil hydraulic properties (Ni et al., 2019; Leung et al., 2018). Root reinforcement is often quantified by a semi-empirical term called root cohesion (Wu et al.,1979) through observations from almost exclusively direct shear tests. In slope application, however, the principal stress directions in soil elements rotate along a slip surface (Zdravković et al., 2002). Observations of direct shear stress paths can only explain the strength behaviour of rooted soils at limited portions of the slip surface (Gao et al., 2021). Importantly, strength anisotropy due to anisotropic soil fabric and the root system cannot be considered. Fabric anisotropy has a remarkable effect on peak shear strength (Karimzadeh et al., 2021). Understanding the strength anisotropy of rooted soils through experimental and theoretical means are needed to facilitate a more reasonable assessment of slope safety.

Some failure criteria for rooted soils have been developed. Early research assumed that all roots break simultaneously at failure (Wu et al.,1979). This assumption is not realistic when roots with different diameters and tensile strength exist in the soil. Fibre bundle models have been developed to model the progressive failure of roots in soil based on their diameters and tensile properties (Pollen & Simon, 2009; Schwarz et al., 2013). Most of these models have been established based on data from direct shear tests and considered the contribution of roots to soil shear strength through root cohesion, whereas the friction angle remains unaffected under the framework of the Mohr–Coulomb failure criterion. These failure criteria are only valid for limited stress paths and cannot be used to predict the strength of rooted soils under general 3-D loading conditions. Specifically, these failure criteria cannot capture the effect of root reinforcement anisotropy and the magnitude of the intermediate principal stress.

Few attempts have been made in modelling the strength anisotropy of rooted soils. However, some developments have been made in the anisotropic failure criteria of fibre-reinforced soils (FRSs), the internal structure of which has some similarities to that of rooted soils (e.g. Michalowski & Cermák, 2002; Diambra et al., 2010; Gao & Zhao, 2013). Although FRS and rooted soil share similar load transfer mechanisms under certain circumstances (i.e. through the mobilisation of interfacial friction and the tensile strength of fibres or roots), existing failure criteria for FRS cannot be directly applied to rooted soils because they have some major differences: (a) the tensile properties of roots depend upon root diameter and water content (e.g., Boldrin et al., 2017, 2018b; Wu et al., 2021). For examples, the tensile strength of hydrated vetiver roots with a diameter of 0.1 and 1.7 mm was 96 MPa and 20 MPa, respectively (Wu et al., 2021), while the tensile strength of dry and hydrated roots, both at the same diameter of 0.15 mm, can differ by 5 MPa (Wu et al., 2021). On the other hand, the tensile properties of fibres for a given material are constant [e.g. 700 MPa for polypropylene (PP; Correia et al., 2021) and 1250 MPa for glass fibres (Maher & Gray, 1989)]; (b) roots can have a larger aspect ratio. For instance, a root with a given diameter (in millimetre scale) can be several meters long (Malamy, 2005; Bengough et al., 2006), but fibres typically have an aspect ratio ranging between 40 to 100 (Michalowski & Čermák, 2002; Soltani et al., 2018); and (c) roots have varying diameters and are interconnected (Malamy, 2005; Bengough et al., 2006), whereas fibres have constant diameter and are individual and not interconnected (Michalowski & Cermák, 2002; Diambra et al., 2010). These existing failure criteria consider that the strength anisotropy of FRS is associated with the inclusion of fibres, whereas the fabric anisotropy of soil is ignored (Michalowski & Cermák, 2002; Diambra et al., 2010; Gao & Zhao, 2013). However, Karimzadeh et al. (2022) who applied an energy-based approach to interpret the undrained triaxial behaviour of artificial soil–root composite showed that the fabric anisotropy of the host soil plays a critical role in the strength anisotropy of rooted soils. Moreover, the anisotropic behaviour of rooted soils is different from that of FRS because of the different sample preparation methods adopted. For examples, moist or vibration tamping would result in an isotropic fabric (i.e., no obvious preferential particle orientation) of FRS (Diambra et al., 2010; Soriano et al. 2017) because particle aggregates are constrained by matric suction in initially unsaturated samples (Ni et al.,2021). Samples produced by dry deposition method where moisture is absent, on the other hand, would have more anisotropic fabric (Miura & Toki 1982; Vaid et al. 1999) for the rooted soils. Moreover, there are fundamental differences in the distribution and orientation between roots and fibres in the soil. While root growth and hence root orientation primarily depend on plant species and environmental conditions (Bengough et.al, 2006), owing to sample preparation (moist or vibration tamping), most of the fibres would be oriented sub-horizontally in the soil (i.e. ±π/4; Michalowski and Čermák, 2002). Thus, developing anisotropic failure criteria specific to rooted soils considering the anisotropy induced by roots and host soil simultaneously is important.

The objective of this study was to develop a 3-D anisotropic failure criterion for rooted soils. Fabric tensors for the internal structure of the host soil and root system were employed in the failure criterion. Two series of consolidated drained triaxial tests, following compression and extension stress paths, were conducted to study the shear strength of bare and rooted soils at different overconsolidation ratios (OCRs) and effective confining pressures. The new failure criterion was used to predict the test data and shear strength of rooted soils under general 3-D loading conditions.

Theoretical modelling

Definition of microstructure fabric tensor of rooted soil

Microstructure fabric tensors have been used to characterise soil anisotropy (Tobita, 1988; Pietruszczak & Mroz, 2000). It is a tensor that measures material fabric associated with, for instance, the arrangement of intergranular contacts and the fracture distribution in the damaged material (Pietruszczak & Mroz, 2001). The microstructure fabric tensor of bare soil can be expressed as:

$$F_{ij} = \begin{bmatrix} F_2 & 0 & 0 \\ 0 & F_1 & 0 \\ 0 & 0 & F_3 \end{bmatrix} = \eta_{\circ|B}\left(\begin{bmatrix} \Omega_{2|B} & 0 & 0 \\ 0 & \Omega_{1|B} & 0 \\ 0 & 0 & \Omega_{3|B} \end{bmatrix} + \begin{bmatrix} 1 & 0 & 0 \\ 0 & 1 & 0 \\ 0 & 0 & 1 \end{bmatrix}\right), \qquad 1$$

where F_1, F_2 and F_3 are the principal values of F_{ij}; $\eta_{\circ|B} = (F_1 + F_2 + F_3)/3$ is the mean of the principal values, which indicates the average of material properties in different directions; and $\Omega_{1|B}$, $\Omega_{2|B}$ and $\Omega_{3|B}$ are the principal values of the deviatoric part of the tensor, which reflect the degree of anisotropy. The sum of these principal values is zero (i.e., $\Omega_{1|B} + \Omega_{2|B} + \Omega_{3|B} = 0$). The spectral decomposition of the tensor can be represented as follows:

$$F_{ij} = F_1 e_i^{(1)} e_j^{(1)} + F_2 e_i^{(2)} e_j^{(2)} + F_3 e_i^{(3)} e_j^{(3)}, \tag{2}$$

where $e_i^{(\alpha)}$ (α = 1, 2, 3) are the unit vectors representing the principal directions of the fabric tensor (Fig. 1). Given that the anisotropy related to the soil and root system affect the mechanical behaviour of rooted soil, the fabric tensor for root network (R_{ij}) is defined as follows to address the anisotropy arising from root morphology, orientation, surface area of root contact with soil or the combination of different sources of anisotropy on the mechanical behaviour of composite:

$$R_{ij} = \begin{bmatrix} R_2 & 0 & 0 \\ 0 & R_1 & 0 \\ 0 & 0 & R_3 \end{bmatrix} = \eta_{\circ|R} \left(\begin{bmatrix} \Omega_{2|R} & 0 & 0 \\ 0 & \Omega_{1|R} & 0 \\ 0 & 0 & \Omega_{3|R} \end{bmatrix} + \begin{bmatrix} 1 & 0 & 0 \\ 0 & 1 & 0 \\ 0 & 0 & 1 \end{bmatrix} \right) \tag{3}$$

where $\eta_{R\circ}$ is the mean of the principal values of R_{ij}, and $\Omega_{1|R}$, $\Omega_{2|R}$ and $\Omega_{3|R}$ are the principal values of the deviatoric part of the root network tensor.

It is well known that soils have a cross-anisotropic internal structure due to gravity and the compaction process; thus, $F_1 = F_3$. Note that F_1 and F_3 are not necessarily smaller than F_2 (Li & Dafalias, 2002). Some studies show that root morphological traits in soil is also approximately cross-anisotropic in homogenous samples based on the observation of root growth from transparent moulds (Mahannopkul & Jotisankasa, 2019) and the 3-D X-ray scanning of roots in soil (e.g., Mairhofer et al., 2012; Floriana et al., 2021). The isotropic plane for the root network is the same as that for soil, which is typically horizontal; thus, $R_1 = R_3$.

Notably, F_{ij} and R_{ij} are not directly related to the specific sources of anisotropy in soil, such as particle/contact normal distribution or root orientation. They are used as general tensors to characterise the effect of internal structures on the mechanical behaviour of soils. Given that anisotropy introduces different effects on cohesion and friction angle, the cohesive and frictional characteristics of rooted soils are modelled using different principal values for F_{ij} and R_{ij}. Indeed, such definition of fabric tensors have also been used in existing failure criteria (Pietruszczak & Mroz, 2001; Kong et al., 2013; Gao et al., 2021). The advantage of this approach is that the fabric tensors can be determined based on the mechanical properties of the soil, such as shear strength or elasticity (Zhao & Gao, 2016). When a fabric tensor related to a specific source of anisotropy is used, the fabric tensor has to be determined by the measurements of the internal structure, which are typically difficult. Extra model parameters are also needed to describe the effect of anisotropy on soil behaviour (Yang et al., 2008).

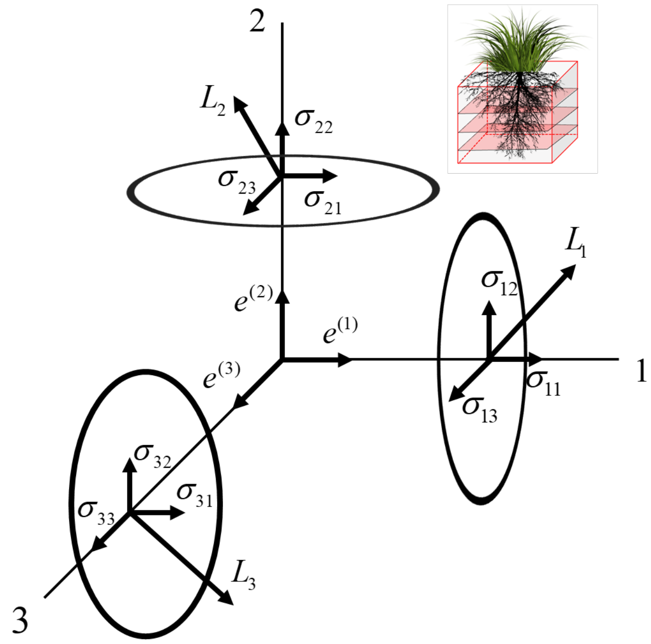

(a)

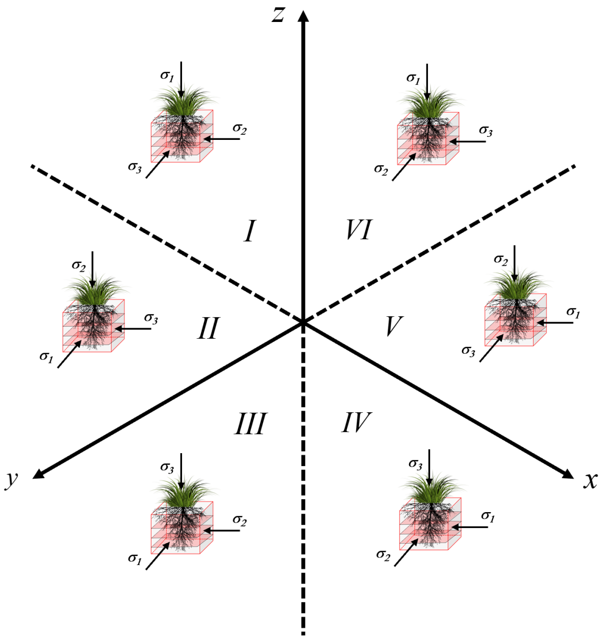

(b)

Figure 1: Schematics of (a) the tractions of loading moduli on the planes normal to a microstructure tensor (after Pietruszczak & Mroz, 2001) and (b) the orientation of principal stresses with respect to soil bedding planes in the six sectors of the π-plane (Lade, 2008).

Framework of anisotropic failure criterion

This study adopted the approach of Pietruszczak & Mroz (2000) to model soil anisotropy as a function of the relative orientation between the axes of principal stress and the microstructure fabric tensor. In this approach, the effect of fabric anisotropy on soil behaviour was addressed using the traction of the stress tensor on the microstructure fabric tensor. Traction is expressed as the mixed invariants of the stress and microstructure fabric tensors (Pietruszczak & Mroz, 2001; Pietruszczak, 2010).

The loading orientation needs to be specified with respect to the direction of the material's microstructure. Figure 1a shows the traction of the loading moduli relative to the principal axes of a microstructure fabric tensor (Pietruszczak & Mroz, 2001; Pietruszczak, 2010). The generalised stress vector based on the magnitudes of the traction of the loading moduli on the planes normal to the axes of F_{ij} (t_i) can be expressed as follows:

$$L_i = t_j e_i^{(j)} \qquad (i, j = 1,2,3), \tag{4}$$

where t_i can be defined as (see also Fig. 1):

$$t_j = \sqrt{\sigma_{j1}^2 + \sigma_{j2}^2 + \sigma_{j3}^2} \qquad (j = 1,2,3). \tag{5}$$

Accordingly, the unit vector that specifies the loading direction is expressed as:

$$l_i = \frac{L_i}{(L_k L_k)^{1/2}} \qquad (i, k = 1, 2, 3). \tag{6}$$

Hence, the anisotropy parameter (η) is defined by the projection of F_{ij} on l_i via the quadratic form of F_{ij}:

$$\eta = F_{ij} l_i l_j = \eta_{\circ|B}(1 + \Omega_{ij|B} l_i l_j). \tag{7}$$

The variable η describes the effect of load orientation relative to the material axes on soil behaviour. The anisotropy parameter is a zero-degree homogeneous function of stress, which means that the magnitude of stress has no effect on the anisotropy parameter (Pietruszczak, 2010). Accordingly, Equation 7 can be rewritten as follows:

$$\eta = \eta_{\circ|B}(1 + \Omega_{1|B} l_1^2 + \Omega_{2|B} l_2^2 + \Omega_{3|B} l_3^2). \tag{8}$$

For a cross-anisotropic material, where $\Omega_{1|B} + \Omega_{2|B} + \Omega_{3|B} = 0$, $\Omega_{1|B} = \Omega_{3|B}$ and $l_1^2 + l_2^2 + l_3^2 = 1$, Equation 8 can be simplified as follows:

$$\eta = \eta_{\circ|B}[1 + \Omega_{1|B}(1 - 3l_2^2)]. \tag{9}$$

For rooted soils, η is composed of the anisotropy arising from the soil structure and the root network and is expressed as follows:

$$\eta = \eta_{\circ|B}(1 + \Omega_{ij|B} l_i l_j) + \eta_{\circ|R}(1 + \Omega_{ij|R} l_i l_j), \quad 10$$

where $\Omega_{ij|B}$ and $\Omega_{ij|R}$ are the principal values of the deviatoric parts of $F_{ij}$and R_{ij}, respectively. For a cross-anisotropic rooted soil, η can be expressed as:

$$\eta = \eta_{\circ|B}[1 + \Omega_{1|B}(1 - 3l_2^2)] + \eta_{\circ|R}[1 + \Omega_{1|R}(1 - 3l_2^2)] \quad 11$$

The loading direction l_2^2, which describes the loading orientation with respect to the anisotropy axes, can be determined from the stress state within the six sectors of the true triaxial (Figure 1b) as follows (Lade, 2008; Kong et al., 2013):

In true triaxial sectors I and VI:

$$l_2^2 = \frac{{\sigma'_z}^2}{{\sigma'_x}^2 + {\sigma'_y}^2 + {\sigma'_z}^2} = \frac{R^2}{R^2 + [b(R-1)+1]^2 + 1}, \quad 12(a)$$

In true triaxial sectors II and V:

$$l_2^2 = \frac{{\sigma'_z}^2}{{\sigma'_x}^2 + {\sigma'_y}^2 + {\sigma'_z}^2} = \frac{[b(R-1)+1]^2}{R^2 + [b(R-1)+1]^2 + 1}, \quad 12(b)$$

In true triaxial sectors III and IV:

$$l_2^2 = \frac{{\sigma'_z}^2}{{\sigma'_x}^2 + {\sigma'_y}^2 + {\sigma_z'}^2} = \frac{1}{R^2 + [b(R-1)+1]^2 + 1}, \quad 12(c)$$

where $b = (\sigma_2 - \sigma_3)/(\sigma_1 - \sigma_3)$ is the intermediate principal stress ratio; $R = \sigma_1/\sigma_3$ is the major stress ratio; σ_1, σ_2 and σ_3 are the major, intermediate and minor principal stress components, respectively. Furthermore σ'_x, σ'_y and σ'_z is the effective principal stress in the x,y and z direction, respectively.

Formulation of the anisotropic failure criterion for rooted soils

The anisotropic failure criterion of rooted soils were developed based on the isotropic failure criterion proposed by Matsuoka & Nakai (1974), also known as the Spatially Mobilised Plane (SMP) criterion. This criterion was established based on the critical shear–normal stress ratio (τ/σ_N) on a SPM where failure is likely to happen. The stress ratio, expressed in terms of stress invariants, for cohesionless soil (Matsuoka & Nakai, 1974) can be defined as follows:

$$\frac{\tau}{\sigma_N} = \sqrt{\frac{I_1 I_2}{9 I_3} - 1}, \quad 13$$

where I_1, $I_2$and I_3 are the first, second and third stress invariants of the stress tensor, respectively, which are defined as follows:

$$I_1 = \sigma_1 + \sigma_2 + \sigma_3, \tag{14}$$

$$I_2 = \sigma_1\sigma_2 + \sigma_2\sigma_3 + \sigma_1\sigma_3, \tag{15}$$

$$I_3 = \sigma_1\sigma_2\sigma_3. \tag{16}$$

Kong et al. (2013) later extended the isotropic SMP failure criteria to anisotropic condition by combining the criteria with η, proposed by Pietruszczak & Mroz (2001), as follows:

$$\frac{\tau}{\sigma_N} = \sqrt{\frac{I_1 I_2}{9I_3} - 1} = \eta = \eta_{\circ|B}[1 + \Omega_{\circ|B}(1 - 3l_2^2)]. \tag{17}$$

For the case of rooted soils, the friction angle depends on various factors, including the contact between roots and soil particles, the effect of root on soil dilatancy, the friction angle of the host soil, root morphology and confining pressure (Veylon et al., 2015; Muir Wood et al., 2016; Karimzadeh et al., 2021). In the present study, these soil–root interaction mechanisms are captured by η in Equation 11. Accordingly, the anisotropic failure criterion to describe the frictional behaviour of rooted soils is proposed as follows:

$$\frac{\tau}{\sigma_N} = \sqrt{\frac{I_1 I_2}{9I_3} - 1} = \eta = m_{\circ|B}[1 + \Omega_{1|B}^{m}(1 - 3l_2^2)] + m_{\circ|R}[1 + \Omega_{1|R}^{m}(1 - 3l_2^2)], \tag{18}$$

where $m_{\circ|\,B}$ and $m_{\circ|\,R}$ is the mean of the principal values for F_{ij} and R_{ij}, respectively; $\Omega_{1|B}^{m}$ and $\Omega_{1|R}^{m}$ is the principal values of the deviatoric part of the F_{ij} and R_{ij} in direction 1 of the bare and rooted soils, repectively, to describe the friction anisotropy; and l_2^2 is the loading direction with respect to the anisotropy axis (Equation 12).

It is well known that rooted soil has cohesion. For cohesive-frictional materials, such as rooted soils, Matsuoka et al. (1990) extended the isotropic SMP criterion by defining the bonding stress ($\sigma_\circ$) and translating the principal stresses from the intercept of the axes to the origin of axes based on $\sigma_\circ$ (i.e. denoted as $\bar{\sigma}_1$, $\bar{\sigma}_2$ and $\bar{\sigma}_3$); hence, the stress invariants $\bar{I}_1$, $\bar{I}_2$ and $\bar{I}_3$ are as follows:

$$\sigma_\circ = c\cot\varphi, \tag{19}$$

$$\bar{\sigma}_i = \sigma_i + \sigma_\circ \quad (i = 1, 2, 3), \tag{20}$$

$$\bar{I}_1 = \bar{\sigma}_1 + \bar{\sigma}_2 + \bar{\sigma}_3, \tag{21}$$

$$\bar{I}_2 = \bar{\sigma}_1\bar{\sigma}_2 + \bar{\sigma}_2\bar{\sigma}_3 + \bar{\sigma}_1\bar{\sigma}_3, \tag{22}$$

$$\bar{I}_3 = \bar{\sigma}_1\bar{\sigma}_2\bar{\sigma}_3, \tag{23}$$

where c is the cohesion and φ is the internal friction angle. Both variables are dependent on the loading direction and *b* value. Note that Equation 19 has been used for bare soil. Bonding stress is used as a single term that is affected by the fabric anisotropy of rooted soils.

Formulating $\sigma_{\circ}$ for rooted soils requires an understanding of the soil–root interaction. Upon shearing, the relative soil–root displacement mobilises the interfacial shear resistance and root tensile strength. As the roots develop tensile stress, the soil effective stress increases whereas the soil shear stress decreases, which result in an increase in the shear strength of the rooted soil through cohesion. Thus, the cohesion of rooted soils should be a function of friction angle and confining pressure. Furthermore, roots act as a ‘bonding agent’ as they entangle soil particles, which provides an apparent increase in cohesion; this kind of bonding effect is much more pronounced for plants that have a fibrous root system (De Baets et al., 2008; Muir Wood et al., 2016). Root reinforcement (i.e. increase in soil shear strength due to roots) is considered anisotropic and depends on the principal stress directions owing to the anisotropy associated with root distribution in soil. Indeed, as supported by existing studies on the behaviour of rooted soils under triaxial compression and extension paths (e.g. Neto & Mahler, 2017; Karimzadeh et al., 2021), the shear strength of rooted soil depends on the differences in the directions between the major principal stresses and roots. Furthermore, it is important to note that roots reinforce soil differently from fibres. Fibres distributed in the soil are isolated (i.e. not connected); therefore, the load transfer mechanism between soil and fibres is by friction (Gray & Ohashi, 1983; Michalowski, 2008). Thus, the reinforcement effect of fibres decreases as the confining pressure is reduced and eventually diminishes at zero confinement. By contrast, roots are interconnected and would entangle the soil, creating an apparent bonding between soil particles. The presence of roots is believed to provide cohesion to the soil at zero confinement (Muir Wood et al., 2016). Moreover, the cohesion of rooted soil depends on confinement. Specifically, the cohesion is reduced with the decrease in confining pressure, although it does not reach zero owing to the root bonding effects. At high confining pressure, the failure envelope of FRS is asymptotic to a failure line in the effective stress space; this implies that cohesion and friction angle of the failure criterion are independent of confinement. The failure of FRS at high confinement is dictated by fibre yielding or breakage (Gray & Ohashi, 1983; Zornberg, 2002; Michalowski, 2008; Gao & Zhao, 2013). The behaviour of rooted soils are expected to be different from that of FRS at high confinement because (1) the tensile strength of roots is much lower than that of fibres, (2) the length of each root is much greater than that of fibres, and (3) the distribution of roots (which are interconnected) is different from that of fibres. Indeed, Karimzadeh et al. (2021) demonstrated that the presence of roots does not noticeably affect soil shear strength at a confining pressure higher than 100 kPa in undrained triaxial tests on dilative sand following the compression and extension stress paths.

On the basis of the above discussion, a new equation with a similar mathematical form to Equation 11 is proposed to describe the influence of loading direction on the bonding stress $\sigma_\circ$ of rooted soils as follows:

$$\sigma_\circ = c_{\circ|\,B}[1 + \Omega^c_{1|B}(1 - 3l_2^2)] + c_{\circ|\,R}[1 + \Omega^c_{1|R}(1 - 3l_2^2)], \qquad 24$$

where $c_{\circ|\,B}$ and $c_{\circ|\,R}$ are the average cohesion values of bare and rooted soils, respectively, and $\Omega^c_{1|B}$ and $\Omega^c_{1|R}$ describe the degree of deviatoric anisotropy in cohesion caused by the host soil and root system, respectively (Equation 12). $c_{\circ|\,R}$ and $\Omega^c_{1|R}$ in Equation 24 are different from $m_{\circ|\,R}$ and $\Omega^m_{1|R}$ in Equation 18 given the fundamental differences in the contributions of cohesion and friction angle to the shear strength of rooted soils (Pietruszczak & Mroz, 2001).

Triaxial tests

Materials and sample preparation

Completely decomposed granite (CDG) was sourced from a construction site in Hong Kong for testing. The soil was sieved to 2 mm prior to sample preparation. It is classified as silty sand soil according to the Unified Soil Classification System (ASTM D2487). Some soil index properties are summarised in Table 1. The oven-dried soil was mixed with de-aired water to achieve an optimum water content of 12.6% (by mass), and the moist soil was then sealed and kept in a temperature-controlled room for moisture equalisation for 12 h. Triaxial specimens with 76 mm diameter and 200 mm height were produced by static compaction in 10 layers following the procedures used by Ladd (1977) to ensure uniformity. The target initial dry density was 1488 kg/m^3, which corresponds to 80% of the maximum dry density of the soil.

Table 1: Index test results of completely decomposed granite

Index tests	
Standard compaction test	
Maximum dry density (kg/m^3)	1860
Optimum water content (%)	12.6
Grain size distribution	
Gravel (>4.75 mm)	0
Coarse sand (4.75–2 mm)	0
Medium sand (0.425– 2 mm)	50.67
Fine sand (0.063–0.425 mm)	18.73
Silt (0.063–0.002 mm)	23.49
Clay (<0.002 mm)	6.7
D_{10} (mm)	0.0022
D_{30} (mm)	0.06
D_{50} (mm)	0.43
Coefficient of uniformity (C_u)	309.1
Coefficient of curvature (C_C)	2.4
Liquid limit (%)	27
Plastic limit (%)	24
Plasticity index (%)	3
Specific gravity	2.6
Unified classification	Silty sand (SM)

Vetiver (*Chrysopogon zizanioides* L.) was selected for testing and cultivated in the triaxial samples. Vetiver is an evergreen, gramineous and perennial herbaceous species that is widely found in tropical and subtropical regions, such as India, Malaysia and Hong Kong. Vetiver grass could develop a deep and extensive root system (up to 5 m depth) after 12 months of growth (Mickovski & van Beek, 2009). The tensile elastic modulus, tensile strength at breakage and tensile strain at breakage of the roots of vetiver grass are 344.77±23.81, 26.39±1.05 and 0.249±0.01 mm/mm (mean ± standard error of mean), respectively, at the diameter range of 0.14–1.58 mm (Wu et al., 2021).

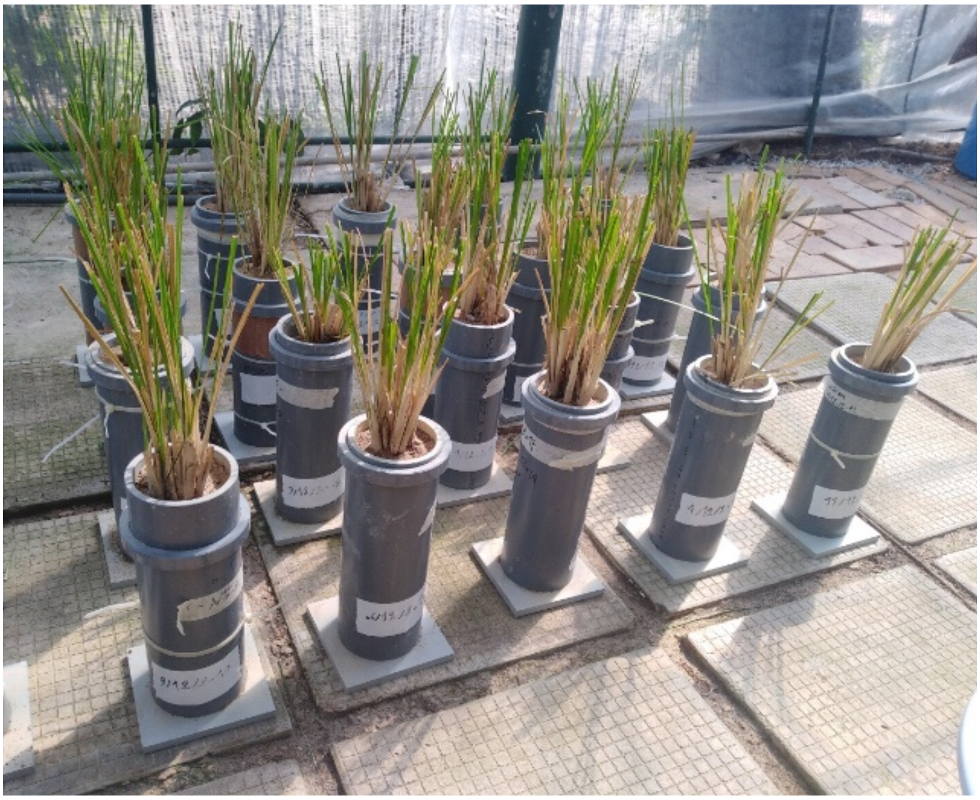

(a)

(b) **(c)**

Figure 2: Images of (a) the planting and growing conditions of vetiver tillers in triaxial moulds in a greenhouse; (b) a triaxial sample mounted on the base pedestal of a triaxial apparatus; and (c) a cross-section of a rooted sample.

Five tillers of vetiver grass were transplanted to the middle of the triaxial samples by burying the roots in a small hole with ~50 mm diameter and ~20 mm depth to produce cultivated samples (Fig. 2a). The cultivated samples were irrigated every day for the first three months after transplanting and then irrigatetd twice a week. The cultivated samples were sent for triaxial testing after growing for 12–15 months (Fig. 2b).

Test plan and procedures

In total, 24 triaxial tests were conducted: 12 for bare soils and 12 for rooted soils. For each type of samples, compression and extension tests were carried out at three effective confining pressures (50, 100 and 150 kPa) to determine the failure envelope and quantify the strength anisotropy. All these tests were repeated for OCR = 3 for both types of samples. The samples were tested at OCR = 3 to investigate the effects of dilatancy on shear strength parameters. Table 2 summarises the test plan.

The samples were mounted on a triaxial apparatus in diameter of 76mm and height of around 155mm and then water-saturated by circulating CO_2 and de-aired water at a small effective confining pressure of 10 kPa to maintain sample stability during the saturation process. Subsequently, a back pressure of at least 80 kPa was applied to the samples to ensure that *b* value was higher than 0.98. Normally consolidated (NC) samples were isotropically consolidated to the desired level of effective confining pressure (i.e. 50, 100 and 150 kPa) and then sheared at an axial strain rate of 0.025%/min under drained condition. The overconsolidated (OC) samples were also isotropically loaded but at much higher levels (150, 300 and 450 kPa). At equilibrium, the samples were subsequently unloaded to 50, 100 and 150 kPa, respectively, to create an OCR of 3 before subjecting the samples to subsequent triaxial compression or extension.

Table 2: Summary of the test program

Test ID	Type of sample	Confining pressure (kPa)	OCR	RVR (%)	Test condition	Stress path
CB50D	Bare	50	1	0	Drained	Compression
CB100D		100	1	0		
CB150D		150	1	0		
EB50D		50	1	0		Extension
EB100D		100	1	0		
EB150D		150	1	0		
CR50D	Rooted	50	1	0.57	Drained	Compression
CR100D		100	1	0.61		
CR150D		150	1	0.67		
ER50D		50	1	0.68		Extension
ER100D		100	1	0.30		
ER150D		150	1	0.37		
CB50D (OCR=3)	Bare	50	3	0	Drained	Compression
CB100D (OCR=3)		100	3	0		
CB150D (OCR=3)		150	3	0		
EB50D (OCR=3)		50	3	0		Extension
EB100D (OCR=3)		100	3	0		
EB150D (OCR=3)		150	3	0		
CR50D (OCR=3)	Rooted	50	3	0.45	Drained	Compression
CR100D (OCR=3)		100	3	0.26		
CR150D (OCR=3)		150	3	0.71		
ER50D (OCR=3)		50	3	0.39		Extension
ER100D (OCR=3)		100	3	0.52		
ER150D (OCR=3)		150	3	0.33		

After testing, all the roots available in the rooted samples were exhumed by gently washing the soil around them (Fig. 3a). A careful inspection suggested that the samples had no observable root breakage. The entire root system exhumed were imaged by a scanner (Model: STD4800, EPSON scanner) and analysed using the Pro-WinRHIZO software to determine relevant root traits, including diameter, length and volume (Fig. 3b). The image analysis result shows that the root system contained some coarse roots with a diameter of 1–2 mm, as well as some extensive finer fiborous roots with a diameter of 0.5–2 mm. The root volume ratio (RVR) of each rooted sample is summarised in Table 2.

(a) **(b)**

Figure 3: Root information of the root system exhumed from a rooted sample (to be sheared upon compression at a confining pressure of 150 kPa in normal consolidation condition): (a) root morphology; (b) a scanned image for determining root traits; root length distribution

Measured shear strength of rooted soils

The shearing behaviours of the bare and rooted samples are shown in Fig. 4. Upon compression ($q > 0$), the presence of roots reduced the shear strength of the NC samples (Fig. 4a) but had little effect on the OC cases (Fig. 4b). Indeed, the major principal stress following the triaxial compression path is parallel to the predominant orientation of the roots; hence, the roots did not remarkably mobilise their tensile properties to resist shearing. The presence of roots created interfaces with soil, and the friction at these interfaces was much smaller than that of the soil particles, which resulted in the reduction in the shear strength of the NC rooted soil. Upon extension ($q < 0$), the shear strength of the rooted soils

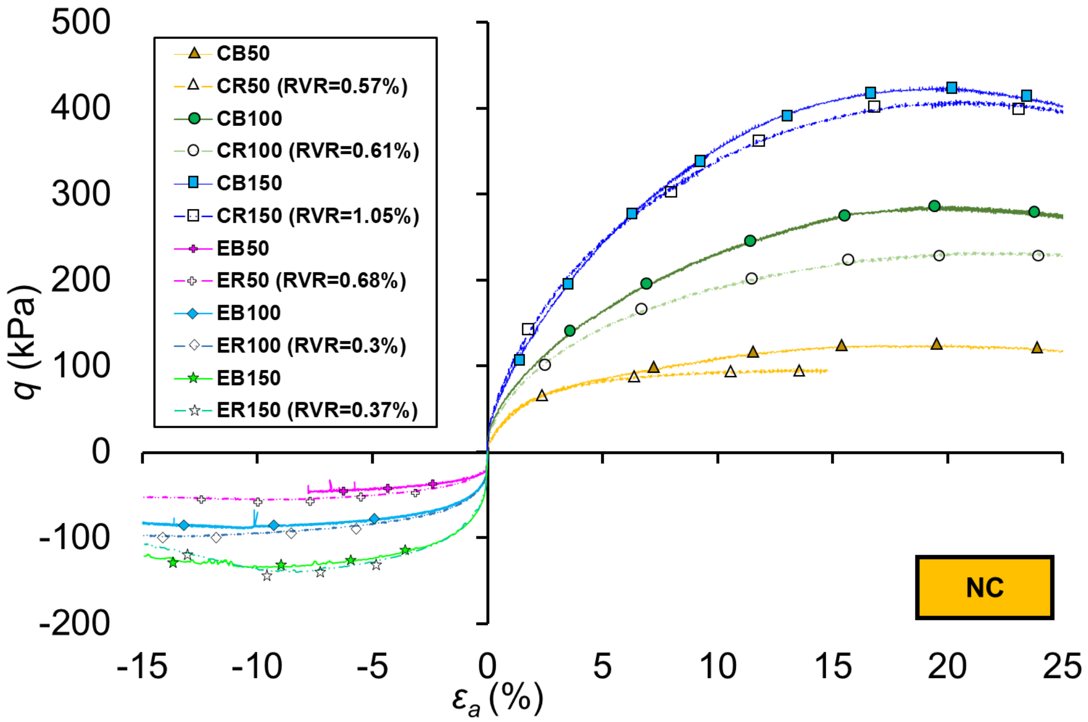

(a)

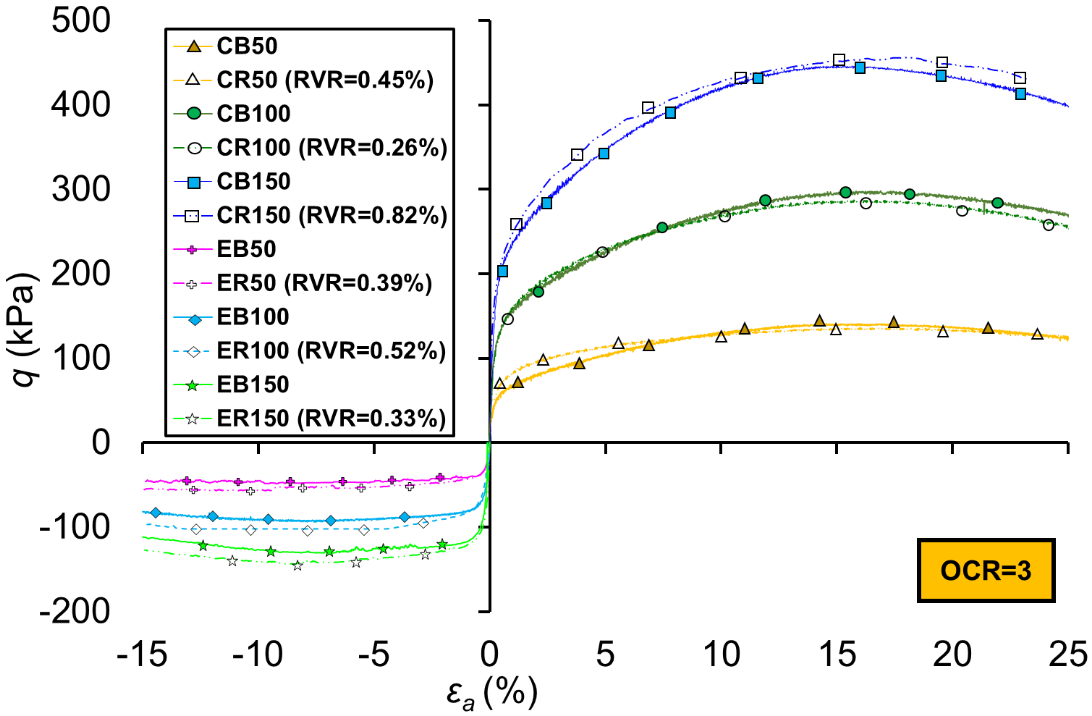

(b)

Figure 4: Shearing behaviours of the bare and rooted soils: (a) NC condition; (b) OC condition (OCR = 3) at p' = 50, 100 150 kPa upon compression and extension paths.

was always higher than that of the bare soils regardless of the OCR because of the substantial mobilisation of the root's tensile properties when the major principal stress was perpendicular to the major orientation of the roots, along which the maximum tensile strain would be mobilised. Evidently, the shear strength of the OC rooted soils was higher than that of the NC case

Figures 5(a) and (b) show the Mohr's circles of the strain rate for the NC and OC rooted samples following triaxial compression and extension, respectively. For the flexible vetiver roots that can transfer only tensions (but not bending), the root tensile strength can be mobilised only in the root segments of which the orientations intersect the tensile section of the Mohr's circle of strain rate upon shearing (Diambra et al., 2013; Muir Wood et al., 2016). The range of intersection can be represented by a geometrical parameter, χ, in these Mohr's circles. Given that χ_{OC} is always equal or larger than χ_{NC}, an increase in OCR shifts the centre of the Mohr's circle of strain (i.e. defined by $\frac{\mathrm{d}\varepsilon_1+\mathrm{d}\varepsilon_3}{2}$) towards the extensive side of the strain increment due to the increase in dilation (Schofield & Wroth, 1968). This shift of the Mohr's circle widens the range of intersection, irrespective of the stress path, explaining the observed higher shear strength for the OC samples compared with the NC case.

The stress paths and the derived failure lines or envelopes for the bare and rooted samples are depicted in Fig. 6. The cohesion and friction angle of the bare soil in the conventional triaxial compression test in section I (denoted as c_{Bc} and ϕ_{Bc}, respectively) were 0 kPa and 36.4°, respectively (Fig. 6a and Table 3). These values are consistent with those reported in the literature for CDG (Wang & Yan, 2006; Yan & Li, 2012). As expected, the compression failure line derived from the NC samples was the same as that for the OC samples. The presence of roots reduced the friction angle (ϕ_{Rc}) of the NC soil by 2°, whereas the cohesion (c_{Rc}) remained unchanged (i.e. 0 kPa, Fig. 6b and Table 3). Overconsolidation appears to introduce an increase in the friction angle of rooted soils.

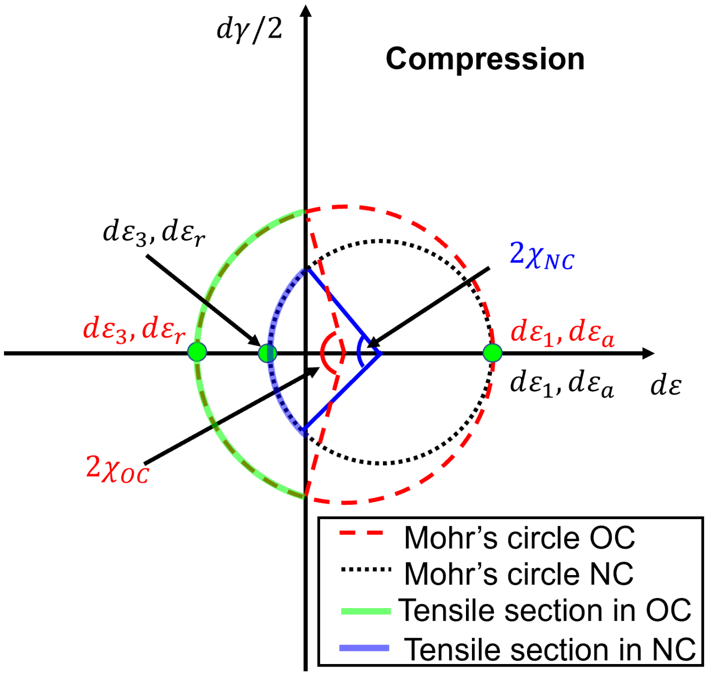

(a)

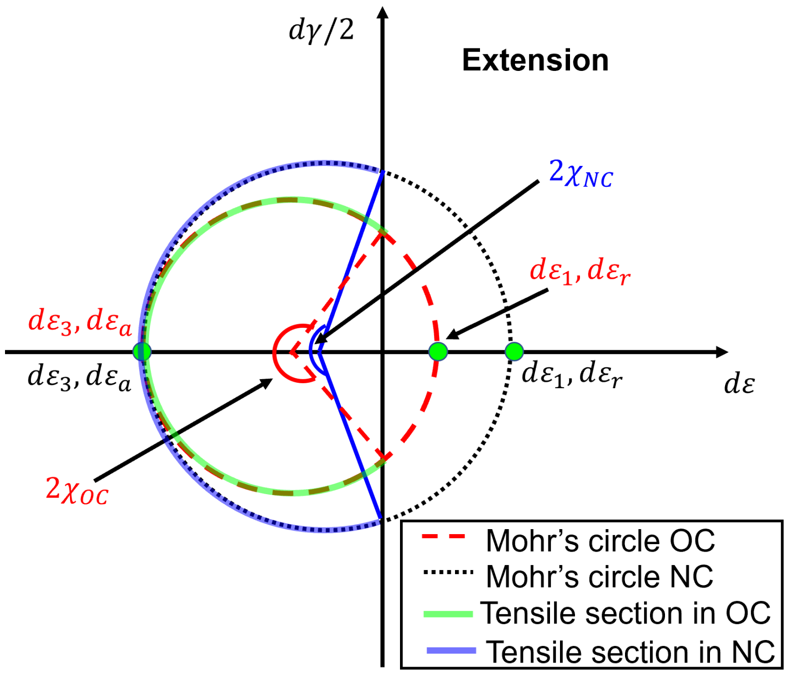

(b)

Figure 5: Shechmatics of the Mohr's circles of strain rate for the triaxial tests of NC and OC rooted samples: (a) compression path and (b) extension path. Note that $d\varepsilon_1$ and $d\varepsilon_3$ are the minor and major principal strain rates, respectively, whereas $d\varepsilon_a$ and $d\varepsilon_r$ are the axial and radial strain rate, respectively

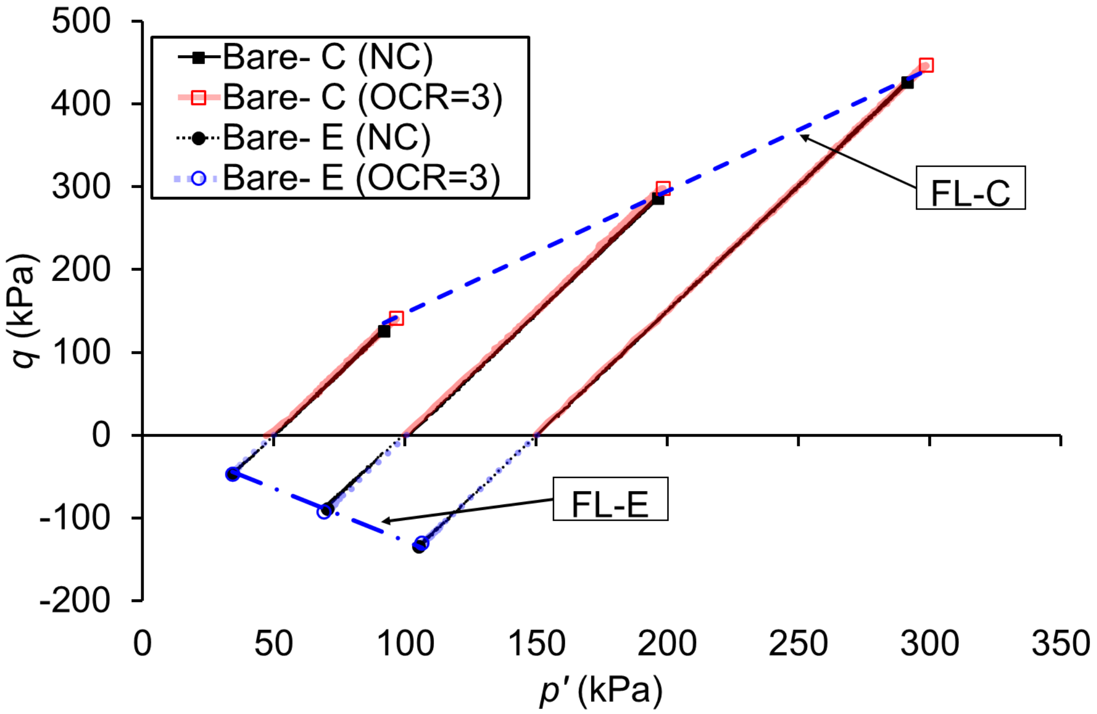

(a)

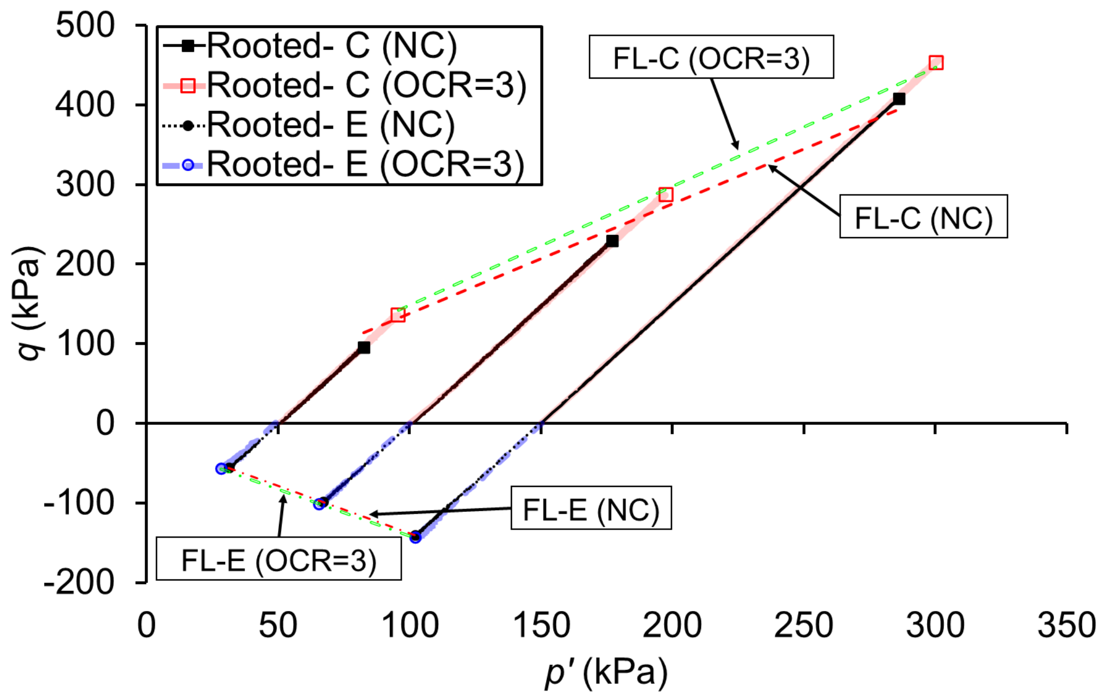

(b)

Figure 6: Stress paths and failure envelopes derived for (a) bare sample and (b) rooted samples at *p*' = 50, 100, 150 kPa under NC and OC conditions.

Table 3: Summary of the shear strength parameters of bare and rooted samples upon triaxial compression and extension paths

Sample type	RVR (%)	M*	ϕ'	c' (kPa)	σ_o' (kPa)
Compression					
Bare	0	1.48	36.4	0	0
Bare (NC)	0	1.45	35.7	0	0
Bare (OCR=3)	0	1.49	36.6	0	0
Rooted (NC)	0.57–0.67*	1.38	34.1	0	0
Rooted (OCR=3)	0.26–0.82	1.48	36.4	0	0
Extension					
Bare	0	1.27	53.7	0	0
Bare (NC)	0	1.28	54.4	0	0
Bare (OCR=3)	0	1.27	53.7	0	0
Rooted (NC)	0.37–0.68*	1.19	47.9	17.2	15.5
Rooted (OCR=3)	0.39–0.52	1.18	47.3	22.3	20.6

*M is the gradient of failure criterion in the $p' - q$ space

Along the conventional triaxial extension path, the friction angle of the bare NC and OC samples (ϕ_{Be}; 53.7°) was higher than the compression case (36.4°) because the difference in σ_2 in the compression and extension paths affect the effective confinement and the anisotropy effects on the dilatancy and soil particle rearrangement during shearing (Ladd et al., 1977, Lade, 2006; Corfdir & Sulem, 2008). However, the presence of roots reduced the friction angle of the rooted soils (ϕ_{Re}) by 6° for the NC and OC samples, whereas a substantial increase in cohesion (c_{Re}) was identified (i.e. 17.2 kPa for the NC samples and 22.4 kPa for the OC samples, Table 3). Indeed, it is not uncommon to find a lower friction angle in rooted soils (compared with the bare counterpart) from the published data following the stress paths of triaxial compression (Zhang et al., 2010; Hoque et al., 2021) and direct shear (Amiri et al., 2019). There were also studies reporting that the presence of roots has no effect on friction angle following the direct shear stress path (Wu et al.,1979; Ali & Osman, 2008; Jotisankasa & Taworn, 2016) and increases the soil friction angle following the triaxial compression path (Garf et al., 2009, Foresta et al., 2020; Karimzadeh et al., 2021). A more detailed discussion on the effects of stress path on the friction angle of rooted soils is given using the proposed model below.

Model calibration

The first step was to derive the shear strength parameters (i.e. friction angle and cohesion) following the conventional triaxial compression and extension paths for bare soil (ϕ_{Bc}, ϕ_{Be}, c_{Bc}, c_{Be}) and rooted soil (ϕ_{Rc}, ϕ_{Re}, c_{Rc}, c_{Re}) by considering the Mohr–Coulomb theory. Based on the values of these shear strength parameters, the principal stresses (σ_1, σ_2, σ_3) and bonding stresses (σ_0, Equation 19) were calculated at a given mean effective stress (p' or $\bar{I}_1$). The second step was to calculate the invariants of the stress tensor ($\bar{I}_1,\ \bar{I}_2,\ \bar{I}_3$) via Equations 21–23 and subsequently substitute them into Equations 17 and 18. The anisotropy parameters that describe the frictional behaviours of bare and rooted soils ($\eta_{C|B}$, $\eta_{E|B}$, $\eta_{C|R}$, $\eta_{E|R}$) need to be determined. The parameters associated with the F_{ij} of the bare soil (i.e. $m_{\circ|B}$, $\Omega^m_{1|B}$) can be calculated by simultaneously solving the linear equations:

$$\begin{cases}\eta_{C|B} = m_{\circ|B}[1 + \Omega^m_{1|B}(1 - 3l_2^2)]\\ \eta_{E|B} = m_{\circ|B}[1 + \Omega^m_{1|B}(1 - 3l_2^2)]\end{cases}. \qquad 25$$

Similarly, the parameters associated with the R_{ij} of the rooted soil (i.e. $m_{\circ|R}$, $\Omega^m_{1|R}$) can be determined by solving the linear equations:

$$\begin{cases}\eta_{C|R} = m_{\circ|B}[1 + \Omega^m_{1|B}(1 - 3l_2^2)] + m_{\circ|R}[1 + \Omega^m_{1|R}(1 - 3l_2^2)]\\ \eta_{E|R} = m_{\circ|B}[1 + \Omega^m_{1|B}(1 - 3l_2^2)] + m_{\circ|R}[1 + \Omega^m_{1|R}(1 - 3l_2^2)]\end{cases}. \qquad 26$$

It should be noted that $m_{\circ|R}$ and $\Omega^m_{1|R}$ depend on OCR and therefore should be calibrated independently for each OCR and $\bar{I}_1$. Finally, the third step is to calibrate the bonding stress and the associated anisotropy. Given that the cohesion of CDG is usually low or zero (Gao & Zhao, 2012), $c_{\circ|\ B}$ and $\Omega^c_{1|B}$ (Equation 24) were set as zero. For the case of rooted soils, $c_{\circ|R}$ and $\Omega^c_{1|R}$ are determined using $\sigma_{\circ C}$ and $\sigma_{\circ E}$ as follows:

$$\begin{cases}\sigma_{\circ C} = c_{\circ|R}[1 + \Omega^c_{1|R}(1 - 3l_2^2)]\\ \sigma_{\circ E} = c_{\circ|R}[1 + \Omega^c_{1|R}(1 - 3l_2^2)]\end{cases}. \qquad 27$$

The calibrated parameters for the bare and rooted soils at $\bar{I}_1 = 101\,kPa$ are summarised in Table 4.

Table 4: Calibration parameters for bare and rooted samples at $\bar{I}_1 = 101\,Kpa$

Tensor	OCR	Calibration parameters
Microstructure fabric (Friction)	0 & 3	$m_{\circ\|B} = 1.072,\ \Omega^{m}_{1\|B} = 0.212$
Microstructure root network (Friction)	0	$m_{\circ\|R} = -0.182,\ \Omega^{m}_{1\|R} = 0.384$
	3	$m_{\circ\|R} = -0.171,\ \Omega^{m}_{1\|R} = 0.604$
Microstructure fabric for 'smeared' sample (Friction)	0	$m_{\circ\|R(Sm)} = 0.889,\ \Omega^{m}_{1\|R(Sm)} = 0.177$
	3	$m_{\circ\|R(Sm)} = 0.901,\ \Omega^{m}_{1\|R(Sm)} = 0.138$
Microstructure fabric (Cohesion)	3	$c_{\circ\|\ B} = 0,\ \Omega^{c}_{1\|B} = 0$
Microstructure root network (Cohesion)	0	$c_{\circ\|R} = 9.585,\ \Omega^{c}_{1\|R} = 0.622$
	3	$c_{\circ\|R} = 13.053,\ \Omega^{c}_{1\|R} = 0.604$
Microstructure fabric for 'smeared' sample (Cohesion)	0	$c_{\circ\|R(Sm)} = 9.585,\ \Omega^{c}_{1\|R(Sm)} = 0.622$
	3	$c_{\circ\|R(Sm)} = 13.053,\ \Omega^{c}_{1\|R(Sm)} = 0.604$

Model evaluation

Figure 7 shows the comparison of the measured and predicted failure criteria of the NC and OC bare and rooted soils at the $p' - q$ space. Upon compression, the model was able to capture the shrinkage of the failure envelope due to the presence of roots in NC soil and the expansion of the failure envelope as the OCR increased. Indeed, the predicted shear strength of the OC rooted soil was similar to that of the NC (or OC) bare soil. Similarly, upon extension, the model predicted the failure envelope of the bare and rooted soils under NC and OC conditions. An interesting phenomenon captured by the model is that the beneficial effect of roots on enhancing the shear strength of the NC and OC soils was diminished at a confining pressure of >200 kPa. This result can be explained by the mismatch between root and soil strains at high confinements (Diambra & Ibraim, 2015; Muir Wood et al., 2016). In this stress regime, the root strains mobilised by the interfacial friction transmitted from the surrounding soil, which is a function of the mean effective stress, could be greater than the soil strain and thus introduced phenomenon analogues to the negative skin friction known in pile engineering. As a consequence, the roots had no influence on the soil's effective stress and made no contribution to soil reinforcement. Furthermore, the second scenario is that most of the roots in the soil broke into shorter lengths as a result of interfacial shearing at high confining pressure, and these shorter roots lack adequate bonding with soil particles (Muir Wood et al., 2016).

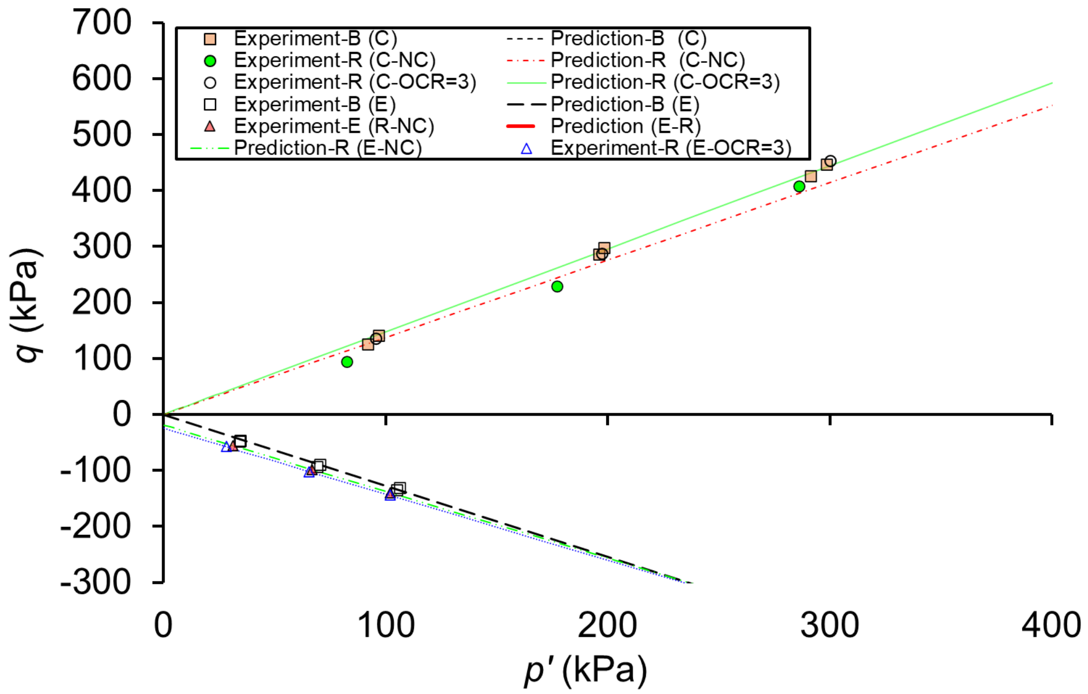

Figure 7: Comparison between the predictions and measurements of the failure envelopes of NC and OC bare and rooted samples.

An alternative modelling of the strength anisotropy of rooted soil may be to treat it as an equivalent composite (i.e. the so called “smeared approach”), without explicitly defining the effect associated with the root network microstructure. In this smeared approach, the same calibration procedures as the bare soil for the microstructure parameters of the cohesion and friction angle were adopted (Table. 4). Although this alternative modelling was able to ‘predict’ the strength anisotropy of rooted soils at both NC and OC cases as depicted in Fig. 8, the parameters calibrated do not have clear physical meaning. Omitting the microstructure root network (R_{ij}) in the modelling would lead to ambiguities when defining the effects of root morphology on the strength anisotropy. Although incorporating R_{ij} in the model requires more calibration effort, this approach returns a more explicit mathematical description of the root effects. Moreover, separating two microstructure fabric tensors (i.e. one for soil skeleton and one for root network) has an advantage to facilitate the development of more physically meaningful constitutive models of rooted soils in the future.

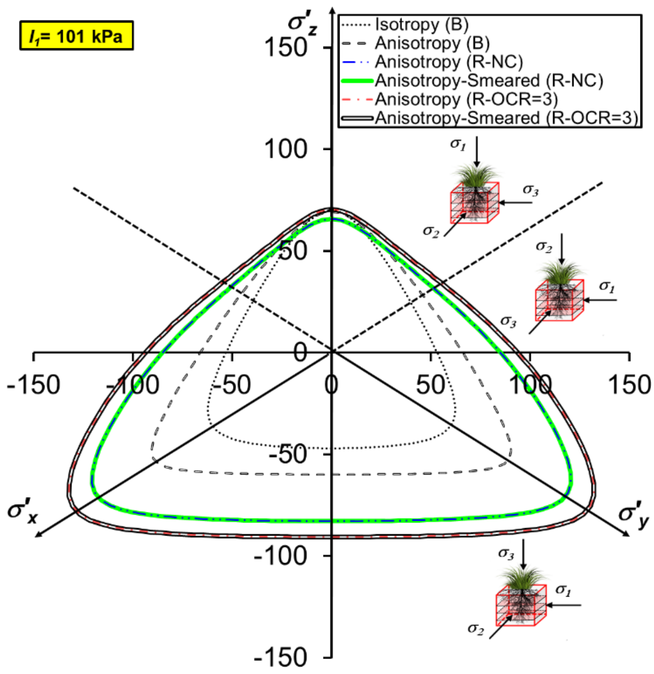

Figure 8: Prediction of the proposed failure criteria in the deviatoric plane of bare soil and rooted soil with and without due consideration of the microstructure root network (R_{ij})

Figure 8 shows the prediction of the anisotropic failure criterion of the rooted soils in the deviatoric plane of 101 kPa at NC and OC conditions with and without due consideration of R_{ij}. The results show that the root reinforcement effect was maximum at sections III and IV of the deviatoric plane but minimum at sections of I and VI. In soil bioengineering application, effective soil reinforcement can be achieved through the strategic positioning of plant species with different root morphologies at different regions of a given failure slip surface. For instance, given a circular failure slip, vetiver grass, whose roots tend to grow predominantly vertically (i.e. 'polyrhizoid'), may be suitable for the regions of failure slip where the stress path follows sections III and IV of the deviatoric plane (e.g. near the slope toe). By contrast, for some regions of failure slip that follow the stress paths in the sections I and VI (e.g. near the slope crest and mid-slope), plant species with a predominant lateral root distribution (i.e. 'oligorhizoid') would be ideal. In this case, the major principal stress is perpendicular to the predominant root direction, having more roots to be orientated along the direction of the soil's tensile strain (refer to Fig. 5). Nonetheless, the plant selection on slopes could be governed by the problems of surface runoff, in addition to the consideration of soil stabilisation (Stokes et al., 2009; De Baets et al., 2008). For example, vetiver grass system has been suggested to plant along the contour lines from the crest to toe for the purpose of reducing surface runoff (Donjadee et al., 2010)

Figure 9 (a) shows the 3-D failure criteria of the bare and rooted soils at the NC and OC conditions for confining pressure lower than 100 kPa. The root reinforcement effects were large at low confinements at all six sections of the deviatoric plane (refer to Fig. 1b) but disminished when exceeding a certain level of confinement (Fig. 9(b)). Indeed, as the confinement increased beyond this level, the associated increase in the shear strength of the bare soil outpaced that of the rooted soil starting from sections I and VI of the deviatoric plane and gradually progressing to the other sections (Fig. 9(c)). Figs. 7 and 9(b) show that the presence of roots did not contribute to the increase in soil shear strength upon any stress path when p' was larger than 200 kPa. Hence, cultivating plants that have similar tensile properties to vetiver roots may not be effective in reinforcing soil when the mean effective stress is high (e.g. >200 kPa), which can possibly be the case under undrained shearing of dilative soils. Karimzadeh et al. (2021) reported that the failure envelope of bare sand and rooted-reinforced sand overlapped at a lower p' of 100 kPa via undrained triaxail extension tests. The difference in the threshold p' beyond which root reinforcement is prohibited may be attributed to the lower elastic modulus and tensile strength of the larger roots (1 mm diameter in Karimzadeh et al. (2021)) compared with those of the smaller roots (0.5 mm with the same length) in the present study. The elastic modulus and tensile strength of synthetic fibres are much greater than those of roots; therefore, a much higher threshold p' is expected in the range of 600–10,000 kPa (Silva Dos Santos et al., 2010 and Kong et al., 2019) in the literature of FRS.

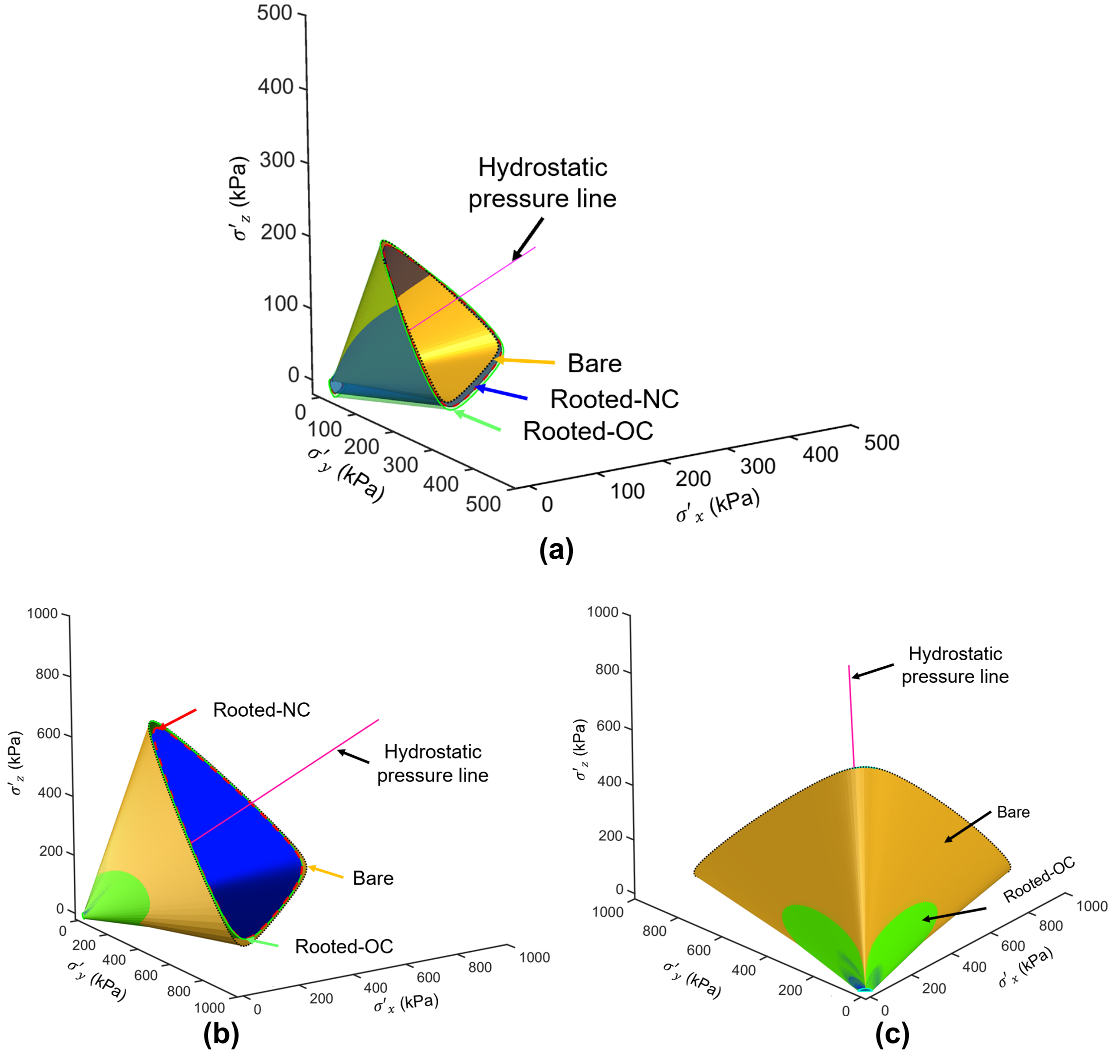

Figure 9: Prediction of the failure criteria of the bare and rooted soils at OCRs of 0 and 3 in a 3-D stress space; (a) for the case with confining pressures lower than 100 kPa; (b) for the case with confining pressure lower than 300 kPa; and (c) rear view of the same failure criteria presented in (b)

Anisotropy of cohesion and friction angle

The cohesion and friction angle of rooted soil are anisotropic and depend on the intermediate principal stress ratio (b). Figure 10a shows the predicted variation in the cohesion of rooted soils at the OCRs of 1 and 3 at the six sections of the deviatoric plane. Notice that the abrupt changes in cohesion and friction angle across the section boundaries did not affect the convexity of the failure criterion (Pietruszczak, 2010). Increasing the OCR increases the cohesion at all sections because of the increase in soil–root contact and the reduction of the contractive behaviour of the soil. The maximum increase in cohesion due to roots occurred at sections III and IV where the roots mobilised the tensile stress the most. The prediction of the friction angles of bare and rooted soils at the six sections of the deviatoric plane are shown in Fig. 10b. At any section, the friction angle of anisotropic bare soil is always higher than the NC (or OC) rooted soils. The maximum difference occurred in sections III and IV, where the roots mobilised

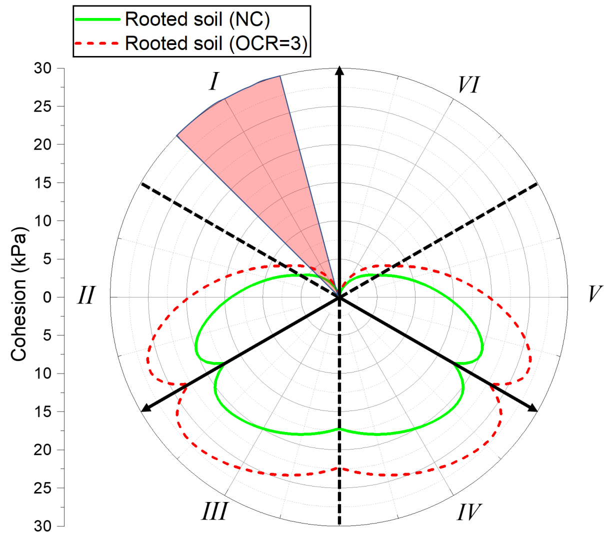

(a)

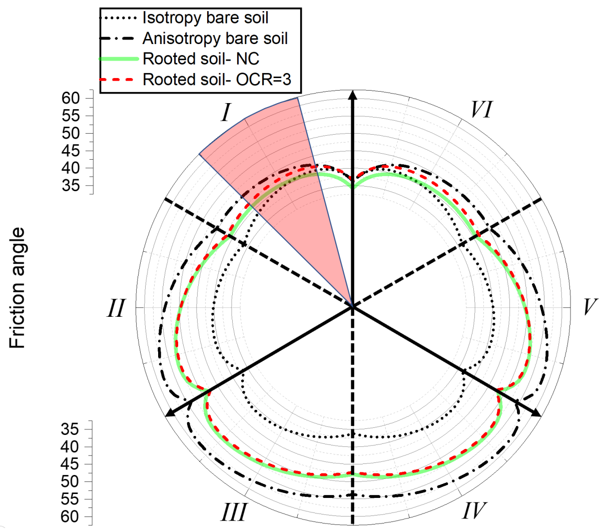

(b)

Figure 10: Prediction of the (a) cohesion and (b) friction angle of bare rooted soils on the deviatoric plane. The shadow zone indicates the possible stress paths following simple shear or direct shear.

their tensile stress is maximum. The friction angles of the NC and OC rooted soils were close to each other, implying that overconsolidation did not introduce change to the friction angle considerably. This outcome might be because the OCR was not high enough to introduce remarkable volumetric dilation to the soil.

In soil bioengineering literature, root reinforcement is often quantified by direct shear test (which is thought to be representative to the shearing condition at the mid-height of a slope). The majority of existing studies concluded that the presence of roots affects cohesion without introducing a substantial influence on the friction angle (Wu et al.,1979; Ali & Osman, 2008; Jotisankasa & Taworn, 2016). Although the exact stress path where rooted samples experienced direct shear conditions could not be identified experimentally, the potential zone of stress regimes (Doherty & Fahey, 2011; Strahler et al., 2018) may be expressed in the deviatoric plan predicted by the model in Fig. 10. Within this zone (i.e. at sections I or VI with a lode angle of ±15°), the difference in cohesion between bare and rooted soils is evident (by 0–5 kPa, Fig. 10a), but the difference in friction angle is minimal (by at most 2°, Fig. 10b). This finding explains why a considerable volume of literature reported that roots affect the cohesion but not the friction angle. Indeed, the potential stress paths of direct (or simple) shear that represents a translation slide in shallow soils are within section I where the effects of soil anisotropy are not evident and the variation in friction angle is almost negligible. Roots causing no/minimal change in soil friction angle is a bold assumption that is valid only for certain stress paths at sections I and VI of the deviatoric plane. Applying this assumption to assess root reinforcement requires a careful examination of the strength anisotropy of rooted soils or, specifically, the root growth pattern with respect to the direction of a failure slip.

Conclusions

This study proposed and verified a new 3-D generalised failure criterion of rooted soils on the basis of the cross-anisotropic SPM failure criterion. The theory of this criterion employed the projection of the microstructure fabric tensors of soil and root network on stress (or strain rate) tensors to address the anisotropic effects of root network and soil fabric on the shear strength parameters of rooted soils upon various effective stress paths. The criterion quantifies the micorstructral properties of soil and roots by eight material parameters that can be obtained by conventional triaxial or torsional shear tests. Twenty-four consolidated drained triaxial compression and extension tests were conducted to determine the model parameters of bare and rooted soils under NC and OC conditions.

The predictions made by the calibrated failure criterion showed that cohesion and friction angle are highly anisotropic and the degree of anisotropy depends on stress paths and the relative orientation of principal stresses and root distribution. The maximum shear strength of rooted soil occurs when roots are orientated along the soil tensile strain, which implies that the major principal stress is perpendicular to the predominated root orientations. An increase in OCR increases the contribution of roots to soil tensile strain, which causes an increase in soil strength. The model explained that following the direct shear path (i.e. at sections I or VI at a lodge angle of ±15° in the deviatoric plane), the effects of soil anisotropy are not evident, and the variation in friction angle is almost negligible, which explains why most of the existing data of direct shear tests showed remarkable changes in cohesion (root cohesion). The proposed anisotropic failure criterion is convex and continuous; thus, it can be employed and integrated into any elastoplastic constitutive model to be developed in the future.

Acknowledgements

The authors acknowledge the financial support provided by the General Research Fund (Grants 16212818, 16202720), the Collaborative Research Fund (Grant C6006-20G) funded by the Hong Kong Research Grants Council and the grant from the National Natural Science Foundation of China (Grant 51922112).

Notation

b	intermediate principal stress ratio
c	cohesion
$c_{\circ\|B}$, $c_{\circ\|R}$	average values of the cohesion of bare and rooted soils
c_{Bc}, c_{Be}	cohesion of bare soil in conventional triaxial compression and extension
c_{Rc}, c_{Re}	cohesion of rooted soil in conventional triaxial compression and extension
OCR	overconsolidation ratio
$e_i^{(\alpha)}$	principal vector of the fabric tensor
F_1, F_2, F_3	principal values of the microstructure fabric tensors

F_{ij}	microstructure fabric tensor
I_1, I_2, I_3	first, second and third stress invariants of the stress tensor
$\bar{I}_1,\ \bar{I}_2,\ \bar{I}_3$	first, second and third translated stress invariants of the stress tensor
L_i	traction of the loading moduli on the planes normal to the axes
l_i	unit vector of loading
$m_{\circ\|\,B}, m_{\circ\|\,R}$	means of the principal values for F_{ij} and R_{ij} in the friction anisotropy
NC	normal consolidated sample
OC	overconsolidated sample
R	major stress ratio
R_1, R_2, R_3	principal values of the root network microstructure tensors
R_{ij}	root network microstructure tensor
RVR	root volume ratio
$d\gamma$	increment of shear strain
$d\varepsilon$	increment of strain
$d\varepsilon_a, d\varepsilon_r$	increments of axial and radial strains
$d\varepsilon_1, d\varepsilon_3$	increments of major and minor strains
η	anisotropy parameter
$\eta_{\circ\|B}, \eta_{\circ\|R}$	means of the principal values of F_{ij} and R_{ij}
$\sigma_\circ$	bonding stress
$\sigma_{\circ C}, \sigma_{\circ E}$	bonding stresses in conventional triaxial compression and extension
$\sigma_1, \sigma_2, \sigma_3$	major, intermediate and minor principal stresses
$\sigma'_x, \sigma'_y, \sigma'_z$	effective principal stress at the x,y and z directions
σ_{ij}	stress tensor
φ	internal friction angle
ϕ_{Bc}, ϕ_{Be}	friction angles of bare soil in conventional triaxial compression and extension
ϕ_{Rc}, ϕ_{Re}	friction angles of rooted soil in conventional triaxial compression and extension
$\Omega_{1\|B}, \Omega_{2\|B}, \Omega_{3\|B}$	principal values of the deviatoric part of F_{ij}
$\Omega_{1\|R}, \Omega_{2\|R}, \Omega_{3\|R}$	principal values of the deviatoric part of R_{ij}

$\Omega^c_{1|B}$, $\Omega^c_{1|R}$ degrees of deviatoric anisotropy in cohesion caused by host soil and root system

$\Omega^m_{1|B}$, $\Omega^m_{1|R}$ principal values of the deviatoric part of the F_{ij} and R_{ij} in friction anisotropy

References

Ali, F. H., & Osman, N. (2008). Shear Strength of a Soil Containing Vegetation Roots. *Soils and Foundations* **48**, No. 4, 587–596, https://doi.org/10.3208/sandf.48.587

ASTM D2487-11. (2018). *Practice for classification of soils for engineering purposes (Unified Soil Classification System)*. *ASTM International*,1–12, https://doi.org/10.1520/D2487-11

ASTM D4767-11D18. (2011). *Test Method for Consolidated Drained Triaxial Compression Test for Soils*. *ASTM International* **i**, No. c, 1–14, https://doi.org/10.1520/D7181

Bengough, A. G., Bransby, M. F., Hans, J., McKenna, S. J., Roberts, T. J., & Valentine, T. A. (2006). Root responses to soil physical conditions; growth dynamics from field to cell. *J. Exp. Bot.* **57**, No. 2 SPEC. ISS., 437–447, https://doi.org/10.1093/jxb/erj003

Boldrin, D., Leung, A. K., & Bengough, A. G. (2017). Root biomechanical properties during establishment of woody perennials. *Ecological Engineering* **109**, 196–206, https://doi.org/10.1016/j.ecoleng.2017.05.002

Boldrin, D., Leung, A. K., & Bengough, A. G. (2018a). Hydrologic reinforcement induced by contrasting woody species during summer and winter. *Plant Soil* **427**, No. 1–2, 369–390, https://doi.org/10.1007/s11104-018-3640-7

Boldrin, D., Leung, A. K., & Bengough, A. G. (2018b). Effects of root dehydration on biomechanical properties of woody roots of Ulex europaeus. *Plant Soil* **431**, No. 1–2, 347–369, https://doi.org/10.1007/s11104-018-3766-7

Consoli, N. C., Festugato, L., & Heineck, K. S. (2009). Strain-hardening behaviour of fibre-reinforced sand in view of filament geometry. *Geosynth. Int.* **16**, No. 2, 109–115, https://doi.org/10.1680/gein.2009.16.2.109

Corfdir, A., & Sulem, J. (2008). Comparison of extension and compression triaxial tests for dense sand and sandstone. *Acta Geotech.* **3**, No. 3, 241–246, https://doi.org/10.1007/s11440-008-0068-x

Correia, N. S., Rocha, S. A., Lodi, P. C., & McCartney, J. S. (2021). Shear strength behavior of clayey soil reinforced with polypropylene fibers under drained and undrained conditions. *Geotext. Geomembranes* **49**, No. 5, 1419–1426, https://doi.org/10.1016/j.geotexmem.2021.05.005

De Baets, S., Torri, D., Poesen, J., Salvador, M. P., & Meersmans, J. (2008). Modelling increased soil cohesion due to roots with EUROSEM. *Earth Surf. Process. Landforms* **33**, No. 13, 1948–1963,

Diambra, A., & Ibraim, E. (2015). Fibre-reinforced sand: interaction at the fibre and grain scale. *Géotechnique* **65**, No. 4, 296–308, https://doi.org/10.1680/geot.14.P.206

Diambra, A., Ibraim, E., Muir Wood, D., & Russell, A. R. (2010). Fibre reinforced sands: experiments and modelling. *Geotextiles and Geomembranes*,**28**, No. 3, 238–250, https://doi.org/10.1016/j.geotexmem.2009.09.010

Diambra, A., Ibraim, E., Russell, A. R., & Muir Wood, D. (2013). Fibre reinforced sands: from experiments to modelling and beyond. *Int. J. Numer. Anal. Meth. Geomech.* **37**, No. 15, 2427–2455, https://doi.org/10.1002/nag.2142

Doherty, J., & Fahey, M. (2011). Three-dimensional finite element analysis of the direct simple shear test. *Comput. Geotech.* **38**, No. 7, 917–924, https://doi.org/10.1016/j.compgeo.2011.05.005

Dos Santos, A. P. S., Consoli, N. C., & Baudet, B. A. (2010). The mechanics of fibre-reinforced sand. *Géotechnique* **60**, No. 10, 791–799, https://doi.org/10.1680/geot.8.P.159

Donjadee, S., Clemente, R. S., Tingsanchali, T., & Chinnarasri, C. (2010). Effects of vertical hedge interval of vetiver grass on erosion on steep agricultural lands. *Land Degrad Dev* **21**, 219–227, https://doi.org/http://dx.doi.org/10.1002/ldr.900

Floriana, A., Andò, E., Viggiani, G., Lenoir, N., Peyroux, R., & Sibille, L. (2021). The use of x-ray tomography to investigate soil deformation around growing roots. *Géotechnique Letters* 11, No. 1, 1–19, https://doi.org/10.1680/jgele.20.00114

Foresta, V., Capobianco, V., & Cascini, L. (2020). Influence of grass roots on shear strength of pyroclastic soils. *Can. Geotech. J.* **57**, No. 9, 1320–1334, https://doi.org/10.1139/cgj-2019-0142

Gao, Z., & Diambra, A. (2021). A multiaxial constitutive model for fibre-reinforced sand. *Géotechnique* **71**, No. 6, 548–560, https://doi.org/10.1680/jgeot.19.P.250

Gao, Z., & Zhao, J. (2012). Efficient approach to characterize strength anisotropy in soils. *J. Eng. Mech.* **138**, No. 12, 1447–1456, https://doi.org/10.1061/(ASCE)EM.1943-7889.0000451

Gao, Z., & Zhao, J. (2013). Evaluation on failure of fiber-reinforced sand. *J. Geotech. Geoenviron. Eng.* **139**, No. 1, 95–106, https://doi.org/10.1061/(ASCE)GT.1943-5606.0000737

Gao, Z., Zhao, J., & Li, X. (2021). The deformation and failure of strip footings on anisotropic cohesionless sloping grounds. *Int J Numer Anal Methods Geomech.* **45**, No. 10, 1526–1545, https://doi.org/10.1002/nag.3212

Graf, Frank, Frei, Martin, & Böll, Albert. (2009). Effects of vegetation on the angle of internal friction of a moraine. *Forest Snow and Landscape Research* **82**, No. 1, 61–77,

Gray, D. H., & Ohashi, H. (1983). Mechanics of fiber reinforcement in sand. *Journal of Geotechnical Engineering* **109**, No. 3, 335–353, https://doi.org/10.1061/(ASCE)0733-9410(1983)109:3(335)

Karimzadeh, A. A., Leung, A. K., Hosseinpour, S., Wu, Z., & Fardad Amini, P. (2021). Monotonic and cyclic behaviour of root-reinforced sand. *Can. Geotech. J.* **58**, No. 12, 1915–1927, https://doi.org/10.1139/cgj-2020-0626

Karimzadeh, A. A., Kwan Leung, A., & Amini, P. F. (2022). Energy-based assessment of liquefaction resistance of rooted soil. *J. Geotech. Geoenviron. Eng.*, **148**, No. 1, 06021016, https://doi.org/10.1061/(ASCE)GT.1943-5606.0002717

Kong, Y., Zhao, J., & Yao, Y. (2013). A failure criterion for cross-anisotropic soils considering microstructure. *Acta Geotech.* **8**, No. 6, 665–673, https://doi.org/10.1007/s11440-012-0202-7

Kong, Y., Zhou, A., Shen, F., & Yao, Y. (2019). Stress–dilatancy relationship for fiber-reinforced sand and its modeling. *Acta Geotech.* **14**, No. 6, 1871–

1881, https://doi.org/10.1007/s11440-019-00834-6

Ladd, R. S. (1977). Specimen preparation and cyclic stability of sands. *ASCE J Geotech Eng Div* **103**, No. 6, 535–547,

Ladd, C, Foot, R, Ishihara, K, Schlosser, F, & Poulos, Harry. (1977). Stress-deformation and strength characteristics. *Proc. 9th Int. Conf. Soil Mech. Found. Eng.* **3**, 421–494,

Lade, P. V. (2006). Assessment of test data for selection of 3-D failure criterion for sand. *Int. J. Numer. Anal. Meth. Geomech.* **30**, No. 4, 307–333, https://doi.org/10.1002/nag.471

Lade, P. V. (2008). Failure criterion for cross-anisotropic soils. *J. Geotech. Geoenviron. Eng.* **134**, No. 1, 117–124, https://doi.org/10.1061/(ASCE)1090-0241(2008)134:1(117)

Leung, A.K., Boldrin, D., Liang, T., Wu, Z.Y., Kamchoom, V. and Bengough, A.G. (2018). Plant age effects on soil infiltration rate during early plant establishment. *Géotechnique* **68,** No. 7, 646-652. https://doi.org/10.1680/jgeot.17.T.037

Leung, A. K., Boldrin, D., Karimzadeh, A. A., & Bengough, A. G. (2019). Role of hydromechanical properties of plant roots in unsaturated soil shear strength. *JGS Special Publication* **7**, No. 2, 133–138, https://doi.org/10.3208/jgssp.v07.020

Li, X. S., & Dafalias, Y. F. (2002). Constitutive modeling of inherently anisotropic sand behavior. *J. Geotech. Geoenviron. Eng.* **128**, No. 10, 868–880, https://doi.org/10.1061/(ASCE)1090-0241(2002)128:10(868)

Liang, T., Knappett, J. A., Bengough, A. G., & Ke, Y. X. (2017). Small-scale modelling of plant root systems using 3D printing, with applications to investigate the role of vegetation on earthquake-induced landslides. *Landslides* **14**, No. 5, 1747–1765, https://doi.org/10.1007/s10346-017-0802-2

Mahannopkul, K., & Jotisankasa, A. (2019). Influences of root concentration and suction on Chrysopogon zizanioides reinforcement of soil. *Soils and Foundations* **59**, No. 2, 500–516, https://doi.org/10.1016/j.sandf.2018.12.014

Maher, M. H., & Gray, D. H. (1989). Satatic response of snds reinforced with ransomly distributed fibres. *J. Geotech. Eng.* **116**, No. 11, 1661–1667, https://doi.org/10.12681/eadd/1834

Malamy, J. E. (2005). Intrinsic and environmental response pathways that regulate root system architecture. *Plant, Cell Environ.* **28**, No. 1, 67–77, https://doi.org/10.1111/j.1365-3040.2005.01306.x

Mairhofer, S., Zappala, S., Tracy, S. R., Sturrock, C., Bennett, M., Mooney, S. J., & Pridmore, T. (2012). RooTrak: automated recovery of three-Dimensional plant root architecture in soil from X-Ray microcomputed tomography images using visual tracking. *Plant Physiol.* **158**, No. 2, 561–569, https://doi.org/10.1104/pp.111.186221

Matsuoka, H., Hoshikawa, T., & Ueno, K. (1990). a general failure criterion and stress-strain relation for granular materials to metals. *Soils and Foundations* **30**, No. 2, 119–127, https://doi.org/10.3208/sandf1972.30.2_119

Matsuoka, H., & Nakai, T. (1974). Stress- deformation and strength characteristics of soil under three different principal stresses. *Proceedings of the Japan Society of Civil Engineers* **1974**, No. 232, 59–70, https://doi.org/10.2208/jscej1969.1974.232_59

Michalowski, R. L. (2008). Limit analysis with anisotropic fibre-reinforced soil. *Géotechnique* **58**, No. 6, 489–501, https://doi.org/10.1680/geot.2008.58.6.489

Michalowski, R. L., & Čermák, J. (2002). Strength anisotropy of fiber-reinforced sand. *Computers and Geotechnics* **29**, No. 4, 279–299, https://doi.org/10.1016/S0266-352X(01)00032-5

Mickovski, S. B., & van Beek, L. P. H. (2009). Root morphology and effects on soil reinforcement and slope stability of young vetiver (Vetiveria zizanioides) plants grown in semi-arid climate. *Plant Soil* **324**, No. 1–2, 43–56, https://doi.org/10.1007/s11104-009-0130-y

Miranda Neto, M. I., & Mahler, C. F. (2017). Study of the shear strength of a tropical soil with grass roots. *Soils and Rocks*, **40**, No. 1, 31–37

Miura, S., & Toki, S. (1982). Sample preparation method and its effect on static and cyclic deformation-strength properties of sand. *Soils Found.* **22**, No. 1, 61–77, https://doi.org/10.3208/sandf1972.22.61

Muir Wood, D., Diambra, A., & Ibraim, E. (2016). Fibres and soils: A route towards modelling of root-soil systems. *Soils Found* **56**, No. 5, 765–778, https://doi.org/10.1016/j.sandf.2016.08.003

Ni, J. J., Leung, A. K., & Ng, C. W. W. (2019). Modelling effects of root growth and decay on soil water retention and permeability. *Can. Geotech. J.* **56**, No. 7, 1049–1055, https://doi.org/10.1139/cgj-2018-0402

Ni, X., Ye, B., Zhang, F., & Feng, X. (2021). Influence of Specimen Preparation on the Liquefaction Behaviors of Sand and Its Mesoscopic Explanation. *J. Geotech. Geoenvironmental Eng.* **147**, No. 2, 04020161, https://doi.org/10.1061/(asce)gt.1943-5606.0002456

Pietruszczak, S. (2010). *Fundamentals of plasticity in geomechanics*. CRC Press, Balkema

Pietruszczak, S., & Mroz, Z. (2000). Formulation of anisotropic failure criteria incorporating a microstructure tensor. *Computers and Geotechnics* **26**, No. 2, 105–112, https://doi.org/10.1016/S0266-352X(99)00034-8

Pietruszczak, S., & Mroz, Z. (2001). On failure criteria for anisotropic cohesive-frictional materials. *Int. J. Numer. Anal. Meth. Geomech.* **25**, No. 5, 509–524, https://doi.org/10.1002/nag.141

Pollen, N., & Simon, A. (2009). Enhanced application of root-reinforcement algorithms for bank-stability modeling. *Earth Surf. Process. Landforms* **34**, No. 4, 471–480, https://doi.org/10.1002/esp.1690

Schofield, A., & Wroth, P. (1968). *Critical state soil mechanics*. McGraw-hill, London, UK, vol. 135

Schwarz, M., Giadrossich, F., & Cohen, D. (2013). Modeling root reinforcement using a root-failure Weibull survival function. *Hydrol. Earth Syst. Sci.* **17**, No. 11, 4367–4377, https://doi.org/10.5194/hess-17-4367-2013

Stokes, A., Atger, C., Bengough, A. G., & Fourcaud, T. (2009). Desirable plant root traits for protecting natural and engineered slopes against landslides. *Plant Soil* **324**, 1–30, https://doi.org/10.1007/s11104-009-0159-y

Stokes, A., Douglas, G. B., Fourcaud, T., Giadrossich, F., Gillies, C., Hubble, T., Kim, J. H., Loades, K. W., Mao, Z., McIvor, I. R., Mickovski, S. B., Mitchell, S., Osman, N., Phillips, C., Poesen, J., Polster, D., Preti, F., Raymond, P., Rey, F., … Walker, L. R. (2014). Ecological mitigation of hillslope instability: ten key issues facing researchers and practitioners. *Plant Soil*

377, No. 1–2, 1–23, https://doi.org/10.1007/s11104-014-2044-6

Soltani, A., Deng, A., & Taheri, A. (2018). Swell-compression characteristics of a fiber-reinforced expansive soil. *Geotext. Geomembranes* **46**, 183–189, https://doi.org/10.1016/j.geotexmem.2017.11.009

Soriano, I., Ibraim, E., Andò, E., Diambra, A., Laurencin, T., Moro, P., & Viggiani, G. (2017). 3D fibre architecture of fibre-reinforced sand. *Granul. Matter* **19**, No. 4, 1–14, https://doi.org/10.1007/s10035-017-0760-3

Strahler, A. W., Stuedlein, A. W., & Arduino, P. (2018). Three-Dimensional Stress-Strain Response and Stress-Dilatancy of Well-Graded Gravel. *Int. J. Geomech.* **18**, No. 4, 04018014, https://doi.org/10.1061/(ASCE)GM.1943-5622.0001118

Tobita, Y. (1988). Yield condition of anisotropic granular materials. *Soils and Foundations* **28**, No. 2, 113–126, https://doi.org/10.3208/sandf1972.28.2_113

Vaid, Y. P., Sivathayalan, S., & Stedman, D. (1999). Influence of specimen-reconstituting method on the undrained response of sand. *Geotech. Test. J.* **22**, No. 3, 187–195, https://doi.org/10.1520/gtj11110j

Veylon, G., Ghestem, M., Stokes, A., & Bernard, A. (2015). Quantification of mechanical and hydric components of soil reinforcement by plant roots. *Can. Geotech. J.* **52**, No. 11, 1839–1849, https://doi.org/10.1139/cgj-2014-0090

Wang, Y. H., & Yan, W. M. (2006). Laboratory studies of two common saprolitic soils in Hong Kong. *J. Geotech. Geoenviron. Eng.* **132**, No. 7, 923–930, https://doi.org/10.1061/(ASCE)1090-0241(2006)132:7(923)

Wu, T. H., McKinnell III, W. P., & Swanston, D. N. (1979). Strength of tree roots and landslides on Prince of Wales Island, Alaska. *Can. Geotech. J.* **16**, No. 1, 19–33, https://doi.org/10.1139/t79-003

Wu, Z., Leung, A. K., Boldrin, D., & Ganesan, S. P. (2021). Variability in root biomechanics of Chrysopogon zizanioides for soil eco-engineering solutions. *Science of The Total Environment* **776**, 145943, https://doi.org/10.1016/j.scitotenv.2021.145943

Yan, W. M., & Li, X. S. (2012). Mechanical response of a medium-fine-grained decomposed granite in Hong Kong. *Engineering Geology* **129–130**, 1–8, https://doi.org/10.1016/j.enggeo.2011.12.013

Yang, Z. X., Li, X. S. & Yang, J. (2008). Quantifying and modelling fabric anisotropy of granular soils . *Géotechnique* **58**, No. 4, 237–248, https://doi.org/10.1680/geot.2008.58.4.237

Yildiz, A., Graf, F., Rickli, C., & Springman, S. M. (2018). Determination of the shearing behaviour of root-permeated soils with a large-scale direct shear apparatus. *Cantena*, **166**, 98–113, https://doi.org/10.1016/j.catena.2018.03.022

Yildiz, A., Graf, F., Rickli, C., & Springman, S. M. (2019). Assessment of plant-induced suction and its effects on the shear strength of rooted soils. *Proceedings of the Institution of Civil Engineers - Geotechnical Engineering* **172**, No. 6, 507–519, https://doi.org/10.1680/jgeen.18.00209

Zdravković, L., Potts, D. M., & Hight, D. W. (2002). The effect of strength anisotropy on the behaviour of embankments on soft ground. *Géotechnique* **52**, No. 6, 447–457, https://doi.org/10.1680/geot.2002.52.6.447

Zhao, J., & Gao, Z. (2016). Unified anisotropic elastoplastic model for sand. *J.*

Eng. Mech., **142**, No. 1, 04015056, https://doi.org/10.1061/(ASCE)EM.1943-7889.0000962

Zornberg, J. (2002). Discrete framework for limit equilibrium analysis of fibre-reinforced soil. *Géotechnique*, **52**, No. 8, 593–604, https://doi.org/10.1680/geot.2002.52.8.593